

Article

Ammonia Plasma-Catalytic Synthesis Using Low Melting Point Alloys

Javishk R. Shah, Joshua M. Harrison and Maria L. Carreon * 

Russell School of Chemical Engineering, The University of Tulsa, 800 S Tucker Dr, Tulsa, OK 74104, USA; jrs943@utulsa.edu (J.R.S.); jmh1756@utulsa.edu (J.M.H.)

* Correspondence: maria-carreon@utulsa.edu; Tel.: +1-918-631-2424

Received: 19 September 2018; Accepted: 30 September 2018; Published: 3 October 2018



Abstract: The Haber-Bosch process has been the commercial benchmark process for ammonia synthesis for more than a century. Plasma-catalytic synthesis for ammonia production is theorized to have a great potential for being a greener alternative to the Haber-Bosch process. However, the underlying reactions for ammonia synthesis still require some detailed study especially for radiofrequency plasmas. Herein, the use of inductively coupled radiofrequency plasma for the synthesis of ammonia when employing Ga, In and their alloys as catalysts is presented. The plasma is characterized using emission spectroscopy and the surface of catalysts using Scanning Electron Microscope. A maximum energy yield of 0.31 g-NH₃/kWh and energy cost of 196 MJ/mol is achieved with Ga-In (0.6:0.4 and 0.2:0.8) alloy at 50 W plasma power. Granular nodes are observed on the surface of catalysts indicating the formation of the intermediate GaN.

Keywords: plasma catalysis; gallium; indium; Ga-In alloys; radiofrequency plasma; ammonia synthesis

1. Introduction

The alternatives to the Haber-Bosch process have been explored for decades. The global production of ammonia will exceed 176 million tons by the end of 2018. Such huge production also accounts for 1–2% of the global greenhouse gas emissions [1,2]. With the growing consciousness as well as the threat of global warming, alternatives to the Haber-Bosch process for ammonia synthesis are not only required for scientific advancement but also as an effort to reduce the effects of global warming.

Ammonia was discovered by Fritz Haber at laboratory scale but the scale-up of the process to an economical scale was performed by Carl Bosch [3]. The early catalysts osmium and uranium used by Haber were replaced with a pure iron metal catalyst by Bosch [4]. The nitrogen is obtained from air and hydrogen is obtained via methane reformation with oxygen from air. The N₂ and H₂ are separated from other gases by refrigeration process and sent to the reactor. The iron catalyst in the reactor helps with the breaking of the dinitrogen triple bond. The ammonia is removed from the exit gas stream via refrigeration [5]. In the terms of formation mechanism, the major energy consumption step for the Haber-Bosch process is the dinitrogen triple bond breaking. Due to the high stability of the dinitrogen triple bond, either high pressure or high temperature is needed. The commercial plants running on the Haber-Bosch process operate at 400–500 °C and 150–250 bar to keep the production economically feasible [5]. This limits the thermodynamic yield for ammonia synthesis to 15%, since at these process conditions the reaction of ammonia formation is reversible. At higher pressure and higher temperature, the decomposition reaction becomes more dominant. The yield can be improved at lower temperatures, but the exothermic nature of the reaction increases the process temperature thus imposing a thermodynamic limit on the ammonia yield [6]. To curb the energy consumption issue, iron catalysts with promoters such as potassium, calcium, and aluminum are employed to break the dinitrogen bond [7].

There have been some advances in the field of alternative pathways for ammonia synthesis. Plasma catalysis has gained attention as an alternative. The discharge is created by exciting the nitrogen and hydrogen molecules, which further break down into charged species, ions, and excited atoms. The already excited species help in shifting the rate-limiting step from breaking of dinitrogen to a surface reaction [8]. In recent years, there have been several reports of ammonia synthesis using dielectric barrier discharge, microwave, glowing arc discharge, and radiofrequency (RF) plasma [9]. Among the most notable reports are Patil et al. (Ru/Tubular Alumina) [10], Iwamoto et al. (metal wool) [11,12], and Kim et al. (Ru/Al₂O₃) [13], all of them performed in a dielectric barrier discharge (DBD). These reports indicated the highest energy yield of ammonia in the range of 5–35 g-NH₃/kWh. The reaction mechanism in a DBD plasma reactor is reasonably understood without a catalyst, but with the introduction of a catalyst it becomes extremely complex [14]. Herein, we focus on tailoring the catalyst for radiofrequency plasma catalytic ammonia synthesis. The catalysts used by other researchers for plasma catalytic ammonia synthesis include Pt,Ni,Fe/Alumina Membrane [15], Ni/SiO₂ [16], Ru/MCM-41 [17], Mo wires [18], MgO [19], CaO, WO₃ [20], and Ru/Carbon nanotube [18,21–24]. The only reports for RF plasma ammonia synthesis were presented by Matsumoto's group with an energy yield of 0.075 g-NH₃/kWh. Moreover, the only catalyst explored by this group was iron and the effect of the catalyst introduction on plasma species was not clearly described. The use of a simple metal catalyst opens the probability of understanding the complex interactions of catalyst and plasma experimentally by studying the point-emission spectra at the metal plasma interface. Pure transition metals have been quite widely studied using molecular simulation for ammonia synthesis [25,26]. However, a novel class of metals and alloys known as low-melting point alloys has been ignored for catalytic applications in experimental as well as simulation reports. Very few reports on the use of molten metals and alloys as catalysts for chemical reactions exist (discussed in the following paragraph).

Raney Ni, a very well-known catalyst, is a Ni rich alloy with Al, developed by Murray Raney in 1929 [27,28]. Since then, alloys have been used as catalysts. Molten metals are postulated to have better activity as compared to solid forms due to higher enthalpy and entropy of the liquid (or semi-liquid) state [29]. Molten metals and alloys have been used as catalysis since the 1970s. Ogino's group has been utilizing molten metal Ga, In, Ti, Pb, Cd, Bi, Sn, and Zn for this purpose. These catalysts were used for dehydrogenation in different organic compounds such as ethers, amines, and alcohols [30–33]. It was stated that a lone pair interaction from oxygen with the molten metal was responsible for the catalytic effect [31]. Another important finding was that there was little decline in catalytic activity for a catalyst used over a year, assuring extremely large catalyst life-cycles [32]. Stelmachowski reported the use of molten metals for pyrolysis of polyolefins and rubber from waste-tires using Zn, Pd, and Sn for the studies. It is noteworthy that he was able to obtain a good yield of liquid hydrocarbons in the range of gasoline and diesel [34,35]. In 2017, Upham et al. reported hydrogen production via methane pyrolysis using molten metal alloys. Interestingly, the catalyst was not poisoned even after several recycles. It was stated that molten alloys worked as bifunctional catalysts. One metal helped in breaking the C–H bond while the other helped in precipitating the carbon, mitigating the poisoning [36]. In recent years, a major application has been the growth of carbon and silicon nanostructures. Specifically, Ga and In have gained attention for this purpose [37–43].

Carreon et al. employed Ga and Ga alloys for the growth of Si nanowires. Pure Ga and Ga-Al alloy presented different reaction kinetics as compared to traditional Au catalyst while the activation energy indicated the difference in catalyst-plasma interaction with the new catalysts [44,45]. Carreon et al. also reported the interaction of hydrogen and nitrogen plasma with gallium. It is essential to note that hydrogen as well as nitrogen species were absorbed into the molten metal, which was strongly inferred by the pressure drop in the chamber. Interestingly, this only happened when the plasma was ignited and not with the neutral gas [46]. From our catalytic results for pure metals, Ga showed the best energy efficiency as well as highest conversion in gentler plasma. Indium has very similar properties to gallium. It forms a MN (metal nitride) similar to gallium and also has a low melting

point. Owing to the enhanced catalytic activity of gallium and other molten metals as well as alloys, it was thought interesting to study the catalytic effect of In and Ga-In alloys. It would not only shed light on the behavior of these low-melting point alloys in plasma but might also help in understanding the driving factor for ammonia yield for pure Ga and In. Also, the melting points of these metals make the alloy preparation and loading easier.

2. Results and Discussion

2.1. Catalytic Activity for Ammonia Synthesis

The catalytic activity was tested for all catalysts at a temperature of 400 °C and pressure of 0.27 torr. As the reflected power was less than 5% of input power, the input power is assumed to be the plasma power. Plasma power is defined as the electrical energy supplied from the power supply to the RF coils. To understand the effect of plasma power, the catalytic activity was tested at 50 W, 150 W, and 300 W. The reactions were repeated twice with standard deviation being less than 2–5%. A total of seven different catalyst compositions were tried. The various alloy compositions and their melting points are represented in Table 1.

Table 1. Composition of various alloys with their melting points.

Gallium Weight %	Indium Weight %	Melting Point (°C) ¹
100	0	29.8
80	20	16.3
60	40	50.2
50	50	61
40	60	65
20	80	90
0	100	156.6

¹ Melting points interpreted from phase diagram in Anderson and Ansara [47].

The molten catalyst was spread on the outside of glass tubes and the tubes were placed in the reaction chamber. The detailed experimental setup is described in Section 3. The temperature of the gas was assumed to be the furnace temperature i.e., 400 °C. To decouple the effect of plasma and thermal energy, a reaction was run at 400 °C without any plasma. Interestingly, no ammonia was detected, which confirms that plasma is the main driving factor for the synthesis of ammonia and the temperature only aids the process. To confirm the catalytic activity of metal coated glass tubes vs. uncoated glass tubes, reactions were run with an empty reaction chamber with uncoated glass tubes in the reaction chamber. There was no difference in the ammonia yield for these sets of reactions. In the manuscript they are referred to as blank reactions. For the complete plot of catalytic activity at different powers for blank reactions, please refer to Figure S1.

The catalytic activity for various alloy compositions at different powers is presented in Figure 1. The steady state ammonia yield is reported in these plots. For ammonia yield (%) vs. time (min) plots for various alloys at different powers, please refer to Figure S2, Figure S3, Figure S4, Figure S5, Figure S6, Figure S7 and Figure S8, in Supporting Information. The order of catalytic activity for Ga and In changes with increase in plasma power. At 50 W and 150 W, pure Ga exhibits better catalytic activity as compared to In, whereas at 300 W, In leads to an ammonia yield 1.5 times higher than employing pure Ga as catalyst. At 50 W, the ammonia yield is slightly higher when a catalyst is employed as compared to blank reactions. As can be observed at 150 W and 300 W, there is a drastic increase in the ammonia yield. This can be attributed to the increase in concentration of excited species with increase in plasma power. At low powers the concentration of excited species is lower. Hence, it can be conjectured that to achieve a significant increase in yields of the final products or to achieve the full potential of a catalyst in plasma reactions, a minimum threshold concentration of excited species must be achieved.

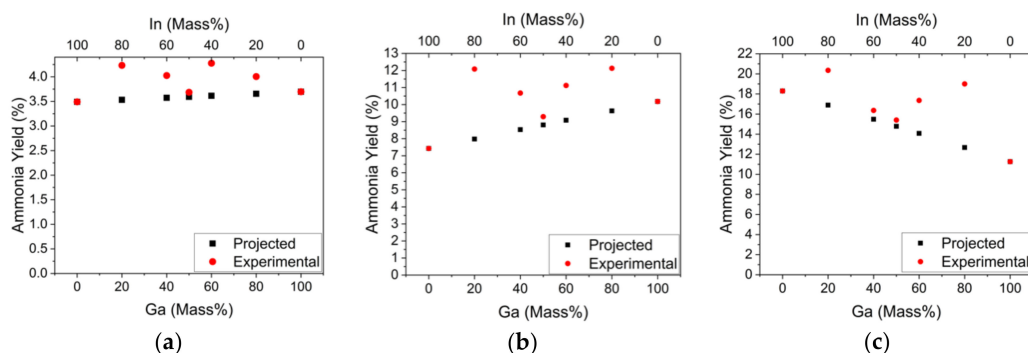


Figure 1. Ammonia yield at steady state (%) vs. alloy composition at various powers (a) 50 W, (b) 150 W, (c) 300 W.

Ideally, it was assumed that the catalytic activity would follow a linear trend as we changed the composition of the alloy. The formula used to determine the projected catalytic activity is represented as Equation (1)

$$X_A = (X_{Ga} * m_{Ga}) + (X_{In} * m_{In}) \quad (1)$$

where X_A = projected ammonia yield for alloy, X_{Ga} = ammonia yield using gallium as catalyst, m_{Ga} = mass fraction of Ga, X_{In} = ammonia yield using indium as catalyst and m_{In} = mass fraction of indium. From experiments, this hypothesis was proven wrong. The alloys show better activity than pure metals. Irrespective of the power used for the reactions, the ammonia yield followed the same trend with change in alloy composition. The catalytic activity follows a bow-type curve instead of a linear one. The bow-type curve (experimental yields) overlaps the linear curve (projected yields) at three points, obviously at the points of pure metals and at equal mass composition i.e., 50:50 for all powers (Figure 1). There are two maxima achieved with varying the alloy composition. The maxima have almost identical yields at a particular power. At 50 W, the maxima are achieved at alloy concentrations of 80:20 and 40:60 (In:Ga) and the maximum yield is 4.5%. The ammonia yield using pure In as catalyst is 3.5% while it is 3.6% with pure Ga. At 150 W, the maxima are achieved at alloy compositions of 80:20 and 20:80 (In:Ga) with the ammonia yield being 12%. The ammonia yields for pure Ga and In as catalysts are 9.8% and 7.3% respectively. At 300 W, the slope of the curve inverted as the ammonia yield with In as the catalyst i.e., 18.1% was higher than ammonia yield with Ga as the catalyst i.e., 11.2%. The maxima are found at alloy compositions of 80:20 and 20:80 (In:Ga) with the ammonia yield being 20%. Interestingly, as the alloy concentration approaches 50:50, the ammonia yields tend to approach the projected yields.

These experiments shed light on the fact that there is some interaction between the metals in the alloys which leads to enhanced catalytic activity as opposed to the pure metals. There is a slight dip in the melting point of the Ga-In phase diagram (see Figure S9). It was hypothesized that it might be a factor for such a catalytic activity trend. Ammonia yields were plotted against the melting points, of the alloys but no pattern emerged (see Figure S10). Daeneke et al. in their review on liquid metals and alloys described in brief the interactions between Ga-In alloys. They found that the alloy properties are highly altered by the composition of the alloy. Specifically, the metallic bonds, free electron density, and plasma frequency (frequency of oscillation of free electron cloud) were determined to be important parameters in determining of the alloy properties for application like energy storage and catalysis. Moreover, indium also acts as an atomic lubricant for free electron clouds to move freely in the alloy [48]. This leads to complex phenomena and interaction between the free electrons in the plasma phase and in the alloys. The electric potential also adds to the dynamics of electron densities and plasma oscillations (also known as Langmuir waves). Hence, it becomes extremely complex to explain the phenomena at quantum or molecular level without simulations, but it does explain the non-linear change in ammonia yield with respect to composition as well as change in catalytic activity order with respect to power. The electron densities in plasma increase as the power increases which increases the

interaction between the free electrons of plasma and the free electrons in alloys. However, to explain the ammonia yield trends, a more simplistic approach using the emission spectra is discussed in the next section.

The energy yields plot for all powers is shown in Figure S11. The highest energy yield observed in this study is 0.31 g-NH₃/kWh with an energy cost of 196 MJ/mol. The energy cost decreased by 20% by using an alloy instead of pure metal while all other parameters were fixed. The energy cost achieved in this study is the lowest as compared to other pure metals employed as catalysts in this study and in our previous publication [49]. Earlier, we reported an energy cost of 237 MJ/mol when Au was used as catalyst in the same reaction system at the same conditions [49]. The present study materializes the potential of molten alloys as catalysts for ammonia synthesis and other plasma-catalytic reactions employing metal catalysts. It unlocks a new range of bimetallic and possible polymetallic materials as catalysts in plasma systems, with the possibility of increasing the energy yield by simply tailoring the catalyst. Moreover, it can help in decreasing the overall cost of the operation by reducing the cost of expensive catalysts like gold or silver by exchanging them with molten alloys, for example gold–gallium alloy, silver–indium alloy, etc.

2.2. Emission Spectroscopy of Plasma

The emission spectra were studied at the same point for all catalysts using a CCD detector and a fiber optic cable. Multiple species were detected in the plasma. There were four nitrogen species detected: N₂ second positive system ($C^3\Pi_u \rightarrow B^3\Pi_g$, 337.1 nm), N₂⁺ first negative system ($B^2\Sigma_u^+ \rightarrow X^2\Sigma_g^+$, 391.4 nm), N₂ first positive system ($B^3\Pi_g \rightarrow A^3\Sigma_u^+$, 662.3 nm), and atomic N ($2p^23p \rightarrow 2p^23s$, 746.8 nm). The hydrogen lines observed at 486.1 nm and 656.3 nm represent H_β and H_α species, respectively. The only NH_x species detected is NH at 336 nm (a pre-shoulder to the N₂ second positive system). The representative spectra for different catalysts are shown in Figure S12, Figure S13 and Figure S14. In our previous work, it was found that H_α species played a major role in determining the ammonia yield when Cu, Pd, Ag, and Au were used as catalysts [49]. The intensities of the H_α species were calculated by processing the data with Origin software package. The intensities are plotted against alloy composition in Figure 2. No clear pattern is observed for 50 W but for 150 W and 300 W, it follows the same trend as ammonia yield with some shift in the maximum concentrations. It can be easily inferred that the H_α species concentration has a direct impact on ammonia yield, but there are also some other factors which regulate the yield. As the intensity of H_α species increases, the ammonia yield also increases which indicates that the pathway for ammonia formation in metals like Cu, Pd, Ag, and Au [49] is different than the pathway for metals like Ga and In. As discussed in the earlier section, there are many more quantum phenomena which involve free electron densities, Langmuir waves, free electron clouds, and the combined conductivity of the alloy at bulk and quantum levels which also have a great impact on the ammonia yield.

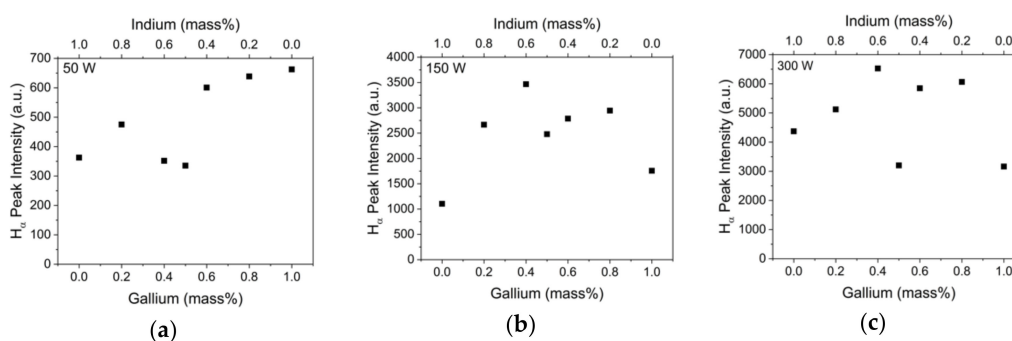


Figure 2. H_α Peak Intensity (a.u.) vs. Alloy Composition (mass%) for various powers (a) 50 W, (b) 150 W and (c) 300 W.

2.3. Characterization of Alloys

The surface of the catalysts underwent some color change which can be observed with the naked eye. Further characterization was carried out using Scanning Electron Microscopy. The SEM images of Ga-In (50:50 wt%) alloy unexposed and exposed to N_2 - H_2 are shown in Figure 3. In the unexposed alloy sample (Figure 3a), it is possible to observe a clean surface with minor irregularities due to rough covering of the glass tubes. On the contrary, the alloy exposed to N_2 - H_2 plasma shows two distinct phases. The left side of the image in Figure 3b is similar to the unexposed sample but the right side has granular nodes on its surface. There is a boundary differentiating both the phases. It was suspected that these granular formations were occurring due to the interaction of N_2 derived species with Ga, which at optimal processing conditions will lead to GaN formation. To validate this hypothesis, experiments were conducted at elevated temperature to support the formation of GaN only in N_2 plasma. Similar granular nodes were observed for short-time synthesis (<15 min) of GaN with gallium coated on glass substrate. At longer times (>60 min), these structures form a more uniform durian-like formation finally converting to GaN nanowires. These durian-like structures have been reported by Nabi et al. [50]. The SEM images of Ga treated in N_2 plasma for various times are shown in Figure S15. The non-uniformity in the samples is due to lower temperature and milder plasma conditions. Carreon et al. reported that hydrogen has a better interaction with Ga as compared to nitrogen [46]. Having a hydrogen-rich environment can result in non-uniformity of these granular nodes on the surface as hydrogen as well as nitrogen derived species competing to interact with the metallic surface. Also, the temperature does not provide enough activation energy for the formation of GaN nano- or micro-structures, for which elevated temperatures are required. When gallium was treated in pure H_2 plasma, no granular nodes were observed. Instead, etching was very dominant.

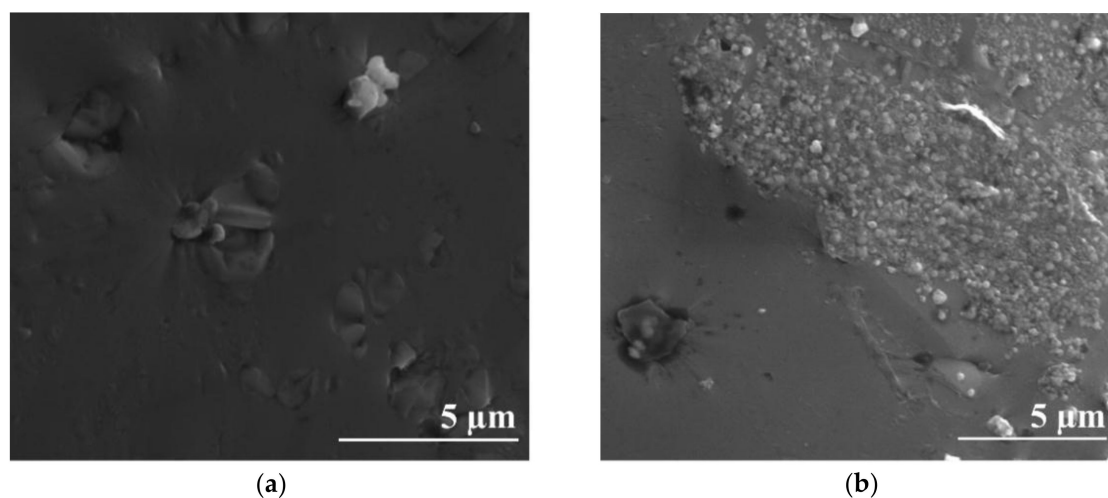


Figure 3. Scanning electron microscope (SEM) images of Ga-In (50:50 wt%), (a) fresh (unexposed to plasma), (b) spent (exposed to N_2 - H_2 plasma).

3. Materials and Methods

The experiments were performed in an in-house built plasma reactor (Figure 4). The reaction was conducted by introducing nitrogen (Praxair, 99%) and hydrogen (Praxair, 99.99%) at a 1:4 N_2 : H_2 ratio to the reaction chamber using mass flow controllers. The nitrogen and hydrogen flow rates were 4 and 16 sccm, respectively. The plasma was ignited using an RF Power Supply with a Matching Network from Seren IPS, Inc. (Vineland, NJ, USA). The typical reaction pressure and temperature were 0.27 torr and 400 °C, respectively. The plasma excitation was started when the furnace reached the desired temperature. The catalysts were coated on inert glass capillaries and loaded in the reactor. The mass of the catalyst loaded was 1 g for all catalysts. The reaction products were bubbled into deionized water. The reactor was uniquely designed for ammonia synthesis by adding an on-line Agilent 7820A

gas chromatograph (GC) (Santa Clara, CA, USA), equipped with a gas sampling valve and HP-PlotQ column (30 m × 0.32 mm × 20 μm). The gases were analyzed every 3 min for 30 min using the GC. All experiments were repeated twice. The experiments were performed for input powers of 50 W, 150 W, and 300 W.

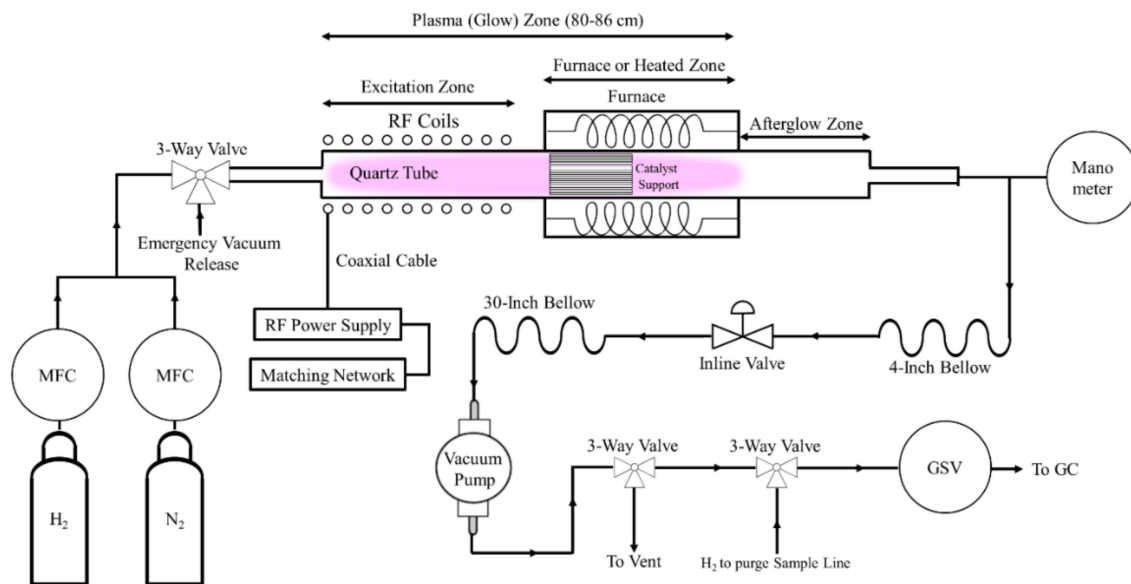


Figure 4. Schematic of the in-house built RF plasma reactor and surrounding equipment for gas inlet and outlet.

The SEM characterization was performed on an FEI Helios NanoLab Scanning Electron Microscope in field emission mode. The emission spectra of plasma were collected with a UV-VIS-NIR spectrophotometer (Avantes ULS3648 series, Louisville, CO, USA) equipped with a dual channel CCD detector. The light was transmitted to the spectrophotometer using a stainless-steel jacketed bifurcated fiber optic cable with a 400 μm fiber. The spectra were collected in the range of 200–1100 nm. The spectral resolution of the spectrophotometer 0.4 nm and grating is 600 lines/mm.

4. Conclusions

Herein, we describe the unusual catalytic behavior of Ga-In alloys for plasma catalytic ammonia synthesis. An increase of 20% is achieved in ammonia energy yield by using an alloy instead of pure metals. There are two optimum compositions of alloys for obtaining maximum ammonia yield for every power. The maximum energy yield of ammonia was obtained at 50 W with catalyst composition of 0.6:0.4 and 0.2:0.8 (Ga:In) having a value of 0.31 g-NH₃/KWh. The emission spectra show the direct dependence of ammonia yield on the concentration of H_α species in the plasma. The SEM characterization shows surface changes on the catalyst due to plasma which are indicative of GaN formation. It is extremely difficult to determine the exact quantum or molecular phenomena experimentally due to involvement of free electron densities and cloud from plasma as well as the alloys. It can be understood more clearly when employing a simulation approach.

Supplementary Materials: The following are available online at <http://www.mdpi.com/2073-4344/8/10/437/s1>, Figure S1: Ammonia Yield (%) vs. Time (min) for reactions run with no catalyst title, Figure S2: Ammonia Yield (%) vs. Time (min) for reactions with pure In as catalyst, Figure S3: Ammonia Yield (%) vs. Time (min) for reactions run with Ga-In Alloy (20:80), Figure S4: Ammonia Yield (%) vs. Time (min) for reactions run with Ga-In Alloy (40:60), Figure S5: Ammonia Yield (%) vs. Time (min) for reactions run with Ga-In Alloy (50:50), Figure S6: Ammonia Yield (%) vs. Time (min) for reactions run with Ga-In Alloy (60:40), Figure S7: Ammonia Yield (%) vs. Time (min) for reactions run with Ga:In Alloy (80:20), Figure S8: Ammonia Yield (%) vs. Time (min) for reactions run with pure Ga as catalyst, Figure S9: Ga-In Alloy Phase diagram, Figure S10: Ammonia Yield (%) vs. Alloy Melting Point (°C) for various plasma powers, Figure S11: Energy Yield (g-NH₃/kWh) vs. Composition of Alloy (mass%) for various plasma powers, Figure S12: Formation of GaN (plasma treatment time), (a) Starting of Nucleation

Process (5 min), (b) Dissolution of Nitrogen in the Gallium Droplet (15 min), (c) Durain-like GaN Nanostructures (30 min), (d) Nanowires of GaN being generated from a single droplet (120 min), Figure S13. XPS Spectra of spent catalyst (pure Ga), Figure S14: Schematic of the in-house built RF plasma reactor and surrounding equipment for gas inlet and outlet, Figure S15: Formation of GaN (plasma treatment time), (a) Starting of Nucleation Process (5 min), (b) Dissolution of Nitrogen in the Gallium Droplet (15 min), (c) Durain-like GaN Nanostructures (30 min), (d) Nanowires of GaN being generated from a single droplet (120 min).

Author Contributions: M.L.C. conceived and directed the presented research. J.R.S. performed the experiments for catalyst preparation and catalytic activity. Synthesis of catalysts and their catalytic performance evaluation was performed at The University of Tulsa. J.M.H. particularly helped in the collection of the catalytic activity data. The paper was written with the contribution of M.L.C., J.R.S., and J.M.H.

Funding: Maria L. Carreon acknowledges the University of Tulsa Faculty Start-up fund, the University of Tulsa Faculty Development Summer Fellowship Program for financial support of this work and the student research grant from the Office of Research and Sponsored Programs at the University of Tulsa.

Conflicts of Interest: The authors declare no conflict of interest

References

1. Tanabe, Y.; Nishibayashi, Y. Developing more sustainable processes for ammonia synthesis. *Coord. Chem. Rev.* **2013**, *257*, 2551–2564. [CrossRef]
2. Global Ammonia Capacity to Reach Almost 250 Million Tons per Year by 2018, says GlobalData. Available online: <https://energy.globaldata.com/media-center/press-releases/oil-and-gas/global-ammonia-capacity-to-reach-almost-250-million-tons-per-year-by-2018-says-globaldata> (accessed on 15 July 2018).
3. Smil, V. *Enriching the Earth: Fritz Haber, Carl Bosch, and the Transformation of World Food Production*; MIT Press: Cambridge, MA, USA, 2004.
4. Kiefer, D.M. Capturing Nitrogen Out of the Air Fritz Haber's high-pressure process for combining nitrogen with hydrogen was a major milestone. *Today's Chem. Work* **2001**, *10*, 117–122.
5. Jennings, J.R. *Catalytic Ammonia Synthesis: Fundamentals and Practice*; Springer: Berlin, Germany, 2013.
6. Modak, J.M. Haber process for ammonia synthesis. *Resonance* **2002**, *7*, 69–77. [CrossRef]
7. Emmett, P.; Brunauer, S. Accumulation of alkali promoters on surfaces of iron synthetic ammonia catalysts. *J. Am. Chem. Soc.* **1937**, *59*, 310–315. [CrossRef]
8. Hong, J.; Prawer, S.; Murphy, A.B. Plasma catalysis as an alternative route for ammonia production: Status, mechanisms, and prospects for progress. *ACS Sustain. Chem. Eng.* **2017**, *6*, 15–31. [CrossRef]
9. Bogaerts, A.; Neyts, E.C. Plasma Technology: An Emerging Technology for Energy Storage. *ACS Energy Lett.* **2018**, *3*, 1013–1027. [CrossRef]
10. Patil, B. Plasma (Catalyst)-Assisted Nitrogen Fixation: Reactor Development for Nitric Oxide and Ammonia Production. Ph.D. Thesis, Eindhoven University of Technology, Eindhoven, The Netherlands, 2017.
11. Aihara, K.; Akiyama, M.; Deguchi, T.; Tanaka, M.; Hagiwara, R.; Iwamoto, M. Remarkable catalysis of a wool-like copper electrode for NH₃ synthesis from N₂ and H₂ in non-thermal atmospheric plasma. *Chem. Commun.* **2016**, *52*, 13560–13563. [CrossRef] [PubMed]
12. Iwamoto, M.; Akiyama, M.; Aihara, K.; Deguchi, T. Ammonia synthesis on wool-like Au, Pt, Pd, Ag, or Cu electrode catalysts in nonthermal atmospheric-pressure plasma of N₂ and H₂. *ACS Catal.* **2017**, *7*, 6924–6929. [CrossRef]
13. Kim, H.H.; Teramoto, Y.; Ogata, A.; Takagi, H.; Nanba, T. Atmospheric-pressure nonthermal plasma synthesis of ammonia over ruthenium catalysts. *Plasma Process. Polym.* **2017**, *14*, 1600157. [CrossRef]
14. Hong, J.; Pancheshnyi, S.; Tam, E.; Lowke, J.J.; Prawer, S.; Murphy, A.B. Kinetic modelling of NH₃ production in N₂-H₂ non-equilibrium atmospheric-pressure plasma catalysis. *J. Phys. D Appl. Phys.* **2017**, *50*, 154005. [CrossRef]
15. Mizushima, T.; Matsumoto, K.; Ohkita, H.; Kakuta, N. Catalytic effects of metal-loaded membrane-like alumina tubes on ammonia synthesis in atmospheric pressure plasma by dielectric barrier discharge. *Plasma Chem. Plasma Process.* **2007**, *27*, 1–11. [CrossRef]
16. Akay, G.; Zhang, K. Process Intensification in Ammonia Synthesis Using Novel Coassembled Supported Microporous Catalysts Promoted by Nonthermal Plasma. *Ind. Eng. Chem. Res.* **2017**, *56*, 457–468. [CrossRef]

17. Peng, P.; Cheng, Y.; Hatzenbeller, R.; Addy, M.; Zhou, N.; Schiappacasse, C.; Chen, D.; Zhang, Y.; Anderson, E.; Liu, Y. Ru-Based Multifunctional Mesoporous Catalyst for Low-Pressure and Non-Thermal Plasma Synthesis of Ammonia. *Int. J. Hydrogen Energy* **2017**, *42*, 19056–19066. [[CrossRef](#)]
18. Tanaka, S.; Uyama, H.; Matsumoto, O. Synergistic effects of catalysts and plasmas on the synthesis of ammonia and hydrazine. *Plasma Chem. Plasma Process.* **1994**, *14*, 491–504. [[CrossRef](#)]
19. Mingdong, B.; Xiyao, B.; Zhitao, Z.; Mindi, B. Synthesis of Ammonia in a Strong Electric Field Discharge at Ambient Pressure. *Plasma Chem. Plasma Process.* **2000**, *20*, 511–520. [[CrossRef](#)]
20. Sugiyama, K.; Akazawa, K.; Oshima, M.; Miura, H.; Matsuda, T.; Nomura, O. Ammonia Synthesis by Means of Plasma over MgO Catalyst. *Plasma Chem. Plasma Process.* **1986**, *6*, 179–193. [[CrossRef](#)]
21. Peng, P.; Li, Y.; Cheng, Y.; Deng, S.; Chen, P.; Ruan, R. Atmospheric Pressure Ammonia Synthesis using Non-Thermal Plasma Assisted Catalysis. *Plasma Chem. Plasma Process.* **2016**, *36*, 1201–1210. [[CrossRef](#)]
22. Uyama, H.; Matsumoto, O. Synthesis of ammonia in high-frequency discharges. II. Synthesis of ammonia in a microwave discharge under various conditions. *Plasma Chem. Plasma Process.* **1989**, *9*, 421–432. [[CrossRef](#)]
23. Uyama, H.; Matsumoto, O. Synthesis of ammonia in high-frequency discharges. *Plasma Chem. Plasma Process.* **1989**, *9*, 13–24. [[CrossRef](#)]
24. Uyama, H.; Nakamura, T.; Tanaka, S.; Matsumoto, O. Catalytic effect of iron wires on the syntheses of ammonia and hydrazine in a radio-frequency discharge. *Plasma Chem. Plasma Process.* **1993**, *13*, 117–131. [[CrossRef](#)]
25. Mehta, P.; Barboun, P.; Herrera, F.A.; Kim, J.; Rumbach, P.; Go, D.B.; Hicks, J.C.; Schneider, W.F. Overcoming ammonia synthesis scaling relations with plasma-enabled catalysis. *Nat. Catal.* **2018**, *1*, 269–275. [[CrossRef](#)]
26. Singh, A.R.; Montoya, J.H.; Rohr, B.A.; Tsai, C.; Vojvodic, A.; Nørskov, J.K. Computational Design of Active Site Structures with Improved Transition-State Scaling for Ammonia Synthesis. *ACS Catal.* **2018**, *8*, 4017–4024. [[CrossRef](#)]
27. Murray, R. Method of Producing Finely-Divided Nickel. U.S. Patents 1,628,190, 10 May 1927.
28. Raney, M. Catalysts from alloys. *Ind. Eng. Chem.* **1940**, *32*, 1199–1203. [[CrossRef](#)]
29. Schwab, G.M. Catalysis on Liquids Metals. *Berichte der Bunsengesellschaft für physikalische Chemie* **1976**, *80*, 746–749. [[CrossRef](#)]
30. Ozawa, S.; Sasaki, K.; Ogino, Y. Reaction of benzyl phenyl ether over various molten metal catalysts. *Fuel* **1986**, *65*, 707–710. [[CrossRef](#)]
31. Okano, K.; Saito, Y.; Ogino, Y. The Dehydrogenation of Amines by Molten Metal Catalysts. *Bull. Chem. Soc. Jpn.* **1972**, *45*, 69–73. [[CrossRef](#)]
32. Saito, Y.; Hiramatsu, N.; Kawanami, N.; Ogino, Y. Dehydrogenation of Some Alcohols by the Molten Metal Catalysts. *Bull. Jpn. Pet. Inst.* **1972**, *14*, 169–173. [[CrossRef](#)]
33. Saito, Y.; Miyashita, F.; Ogino, Y. Studies on catalysis by molten metal: VI. Kinetics and the reaction scheme for the dehydrogenation of isopropyl alcohol over the liquid indium catalyst. *J. Catal.* **1975**, *36*, 67–73. [[CrossRef](#)]
34. Stelmachowski, M. Thermal conversion of waste polyolefins to the mixture of hydrocarbons in the reactor with molten metal bed. *Energy Convers. Manag.* **2010**, *51*, 2016–2024. [[CrossRef](#)]
35. Stelmachowski, M. Conversion of waste rubber to the mixture of hydrocarbons in the reactor with molten metal. *Energy Convers. Manag.* **2009**, *50*, 1739–1745. [[CrossRef](#)]
36. Upham, D.C.; Agarwal, V.; Khechfe, A.; Snodgrass, Z.R.; Gordon, M.J.; Metiu, H.; McFarland, E.W. Catalytic molten metals for the direct conversion of methane to hydrogen and separable carbon. *Science* **2017**, *358*, 917–921. [[CrossRef](#)] [[PubMed](#)]
37. Mukanova, A.; Tussupbayev, R.; Sabitov, A.; Bondarenko, I.; Nemkaeva, R.; Aldamzharov, B.; Bakenov, Z. CVD graphene growth on a surface of liquid gallium. *Mater. Today Proc.* **2017**, *4*, 4548–4554. [[CrossRef](#)]
38. Fujita, J.-I.; Hiyama, T.; Hirukawa, A.; Kondo, T.; Nakamura, J.; Ito, S.-I.; Araki, R.; Ito, Y.; Takeguchi, M.; Pai, W.W. Near room temperature chemical vapor deposition of graphene with diluted methane and molten gallium catalyst. *Sci. Rep.* **2017**, *7*, 12371. [[CrossRef](#)] [[PubMed](#)]
39. Fujita, J.-I.; Miyazawa, Y.; Ueki, R.; Sasaki, M.; Saito, T. Fabrication of large-area graphene using liquid gallium and its electrical properties. *Jpn. J. Appl. Phys.* **2010**, *49*, 06GC01. [[CrossRef](#)]
40. Lee, M.V.; Hiura, H.; Tyurnina, A.V.; Tsukagoshi, K. Controllable gallium melt-assisted interfacial graphene growth on silicon carbide. *Diam. Relat. Mater.* **2012**, *24*, 34–38. [[CrossRef](#)]
41. Lugstein, A.; Steinmair, M.; Hyun, Y.J.; Bertagnolli, E.; Pongratz, P. Ga/Au alloy catalyst for single crystal silicon-nanowire epitaxy. *Appl. Phys. Lett.* **2007**, *90*, 023109. [[CrossRef](#)]

42. Gewalt, A.; Kalkofen, B.; Lisker, M.; Burte, E.P. Gallium Assisted PECVD Synthesis of Silicon Nanowires. *ECS Trans.* **2010**, *28*, 45–56.
43. Pan, Z.W.; Dai, Z.R.; Ma, C.; Wang, Z.L. Molten gallium as a catalyst for the large-scale growth of highly aligned silica nanowires. *J. Am. Chem. Soc.* **2002**, *124*, 1817–1822. [[CrossRef](#)] [[PubMed](#)]
44. Carreon, M.L.; Jasinski, J.; Sunkara, M. Low temperature synthesis of silicon nanowire arrays. *Mater. Res. Express* **2014**, *1*, 045006. [[CrossRef](#)]
45. Carreon, M. Plasma catalysis using low melting point metals. Ph.D. Thesis, University of Louisville, Louisville, KY, USA, 2015.
46. Carreon, M.L.; Jaramillo-Cabanzo, D.F.; Chaudhuri, I.; Menon, M.; Sunkara, M.K. Synergistic interactions of H₂ and N₂ with molten gallium in the presence of plasma. *J. Vac. Sci. Technol. A* **2018**, *36*, 021303. [[CrossRef](#)]
47. Anderson, T.; Ansara, I. The Ga-In (gallium-indium) system. *J. Phase Equilib.* **1991**, *12*, 64–72. [[CrossRef](#)]
48. Daeneke, T.; Khoshmanesh, K.; Mahmood, N.; de Castro, I.; Esrafilzadeh, D.; Barrow, S.; Dickey, M.; Kalantar-Zadeh, K. Liquid metals: Fundamentals and applications in chemistry. *Chem. Soc. Rev.* **2018**, *47*, 4073–4111. [[CrossRef](#)] [[PubMed](#)]
49. Shah, J.; Wang, W.; Bogaerts, A.; Carreon, M.L. Ammonia synthesis by radio frequency plasma catalysis: Revealing the underlying mechanisms. *ACS Appl. Energy Mater.* **2018**, *1*, 4824–4839. [[CrossRef](#)]
50. Nabi, G.; Cao, C.; Khan, W.S.; Hussain, S.; Usman, Z.; Mahmood, T.; Khattak, N.A.D.; Zhao, S.; Xin, X.; Yu, D. Synthesis, characterization, photoluminescence and field emission properties of novel durian-like gallium nitride microstructures. *Mater. Chem. Phys.* **2012**, *133*, 793–798. [[CrossRef](#)]



© 2018 by the authors. Licensee MDPI, Basel, Switzerland. This article is an open access article distributed under the terms and conditions of the Creative Commons Attribution (CC BY) license (<http://creativecommons.org/licenses/by/4.0/>).